SUPERIONS IN THE NARROW NANOPORES WITH MULTIPLE OCCUPANCY

V.N. KHARKYANEN, S.O. YESYLEVSKYY, N.M. BEREZETSKAYA

Department of Physics of Biological Systems,
Institute of Physics, Nat. Acad. of Sci. of Ukraine
(Prosp. Nauky, 46, Kyiv 03039, Ukraine)

PACS 05.20.-y

The general theory of the single-file multiparticle diffusion in narrow pores can be greatly simplified in the case of the inverted bell-like shape of a single-particle energy profile, which is often observed in biological ion channels. There is a narrow and deep groove in the energy landscape of multiple interacting ions in such profiles, which corresponds to the pre-defined optimal conduction pathway in the configurational space. If such a groove exists, the motion of multiple ions can be reduced to the motion of a single quasiparticle, called the superion, which moves in a one-dimensional effective potential. The concept of superions reduces the computational complexity of the problem and provides the very clear physical interpretation of conduction phenomena in narrow pores.

1. Introduction

Narrow nanopores, which conduct ions, are widely known for their unique properties. The particles in narrow pores move in the single-file manner, while the number of particles changes stochastically due to exchange with surrounding solutions. The examples of such pores are the ion channels of biological membranes [1-3] and the carbon nanotubes [4–6].

Narrow nanopores are studied extensively by means of molecular dynamics (MD) [7–9] or Brownian dynamics (BD) [8, 10, 11] simulations. This approach provided insight into the functioning of biological ion channels [8, 11, 12]. However, no general analytical theory of diffusion in narrow pores was available till recently. In our previous work, we presented a theory, which fills this gap [13]. This theory is very general and describes the single-file diffusion of multiple ions in narrow pores under non-equilibrium conditions. The ions move in an arbitrary energy profile, created by the pore walls and the external electrostatic potential and interact explicitly by means of a repulsive potential. Any macroscopic property of the pore (such as a current or a mean occupancy) can be computed providing that these potentials and the concentrations of particles in surrounding solutions are known. It was shown that the problem is reduced to finding the n-particle distribution functions inside the pore $\phi^{(n)}(x_1, ..., x_n; t)$ for all possible occupancies $M \geq n \geq 1$, where M is the maximal number of particles, x_i are the coordinates of the ions.

The problem of finding $\phi^{(n)}(x_1, ..., x_n; t)$ is independent of general analytical derivations and should be solved numerically for each particular system. A quite general way of finding $\phi^{(n)}(x_1, ..., x_n; t)$ was proposed in [13]. The distribution functions $\phi^{(n)}(x_1, ..., x_n; t)$ can be found from the closed hierarchical set of Fokker–Planck equations of increasing dimensionality [13]. We provided the generic computational procedure, which is applicable for an arbitrary single-ion energy profile in the pore. Despite its generality, this procedure remains rather intensive computationally and provides semiquantitative results, as discussed in Section 3.

In the present work, we show that the general analytical theory developed in [13] can be greatly simplified in the case of the specific inverted bell-like shape of a single-ion energy profile, which is observed in real ion channels [9, 13, 14]. The goal of this work is to study general physical principles of the multiparticle diffusion in the potential of this class. We show that the multidimensional distribution functions of the ions inside a pore can be reduced to one-dimensional distribution functions of the quasiparticles (called the superions) in such potentials. All observed macroscopic properties of the pore are then described in terms of the superions. This approximation provides a very simple elegant description

of the pore conductance. It also leads to a very simple efficient numerical procedure of finding $\phi^{(n)}(x_1, ..., x_n; t)$ (providing that the approximation of the superions is valid for a given energy profile).

The idea of superions was already exploited (although in a rather naïve manner) in our previous work [15]. This work provides a much more formal and consistent definition of superions, which is based on the strict general theory developed in [13].

2. The Theory

2.1. The boundary conditions

In the present work, we follow the approach introduced in our general theory [13]. It is assumed that the particle, which crosses the pore boundary and escapes to the solution, loses all correlations with the particles, which remain in the pore abruptly. This means that the probability of reentry of the escaped particle is the same as the probability of entry of any other particle from the solution. As a result, the solutions can be considered as ideal heat baths with given concentrations of particles. This basic assumption leads to the convenient factorization of the probability density function at the channel boundary, which allows describing the events of entry and exit of ions by the simple boundary condition

$$\phi^{(n)}(x_1, ..., x_n; t)\Big|_{x_i = \mp L} =$$

$$= c_{1,2}\phi^{(n-1)}(x_1, ...x_{i-1}, x_{i+1}...x_{n-1}; t), \qquad (1)$$

where $c_{1,2}$ are the concentrations of the ions in solutions, and L is the half-length of the channel. Further details and derivations can be found in [13].

2.2. The energy landscape of a pore

Here, we use a simplified reference model of a pore with inverted bell-like single-ion energy profile. This model was studied extensively in our previous works [13, 15, 18]. The interactions in this model are balanced in such a way that the ions move in a highly concerted manner. Let us formalize this picture. The energy of n ions, which reside in the pore, is

$$U_n(\mathbf{x}) = \sum_{i=1}^{n} U_0(x_i) + \sum_{\substack{i,\, j\,=\,1 \\ (i\,>\,j)}}^{n} V(x_i - x_j), \qquad (2)$$

where U_0 is the single-ion energy profile; V is the repulsive ion-ion interaction potential; x_i is the coordinate of the i-th ion measured along the pore axis; and $\mathbf{x} = \{x_1, x_2, \ldots, x_n\}$, $-L < x_i < L$, where L is the half-length of the pore. The single-file motion of the ions allows us to consider only a part of the whole configurational space, where the ions are ordered from left to right: $G^{(n)} = \{-L \le x_1 \le x_2 \le ... \le x_{n-1} \le x_n \le L\}$.

The single-ion energy profile U_0 has inverted bell-like shape, which can be described by the inverted Gaussian curve

$$U_0(x) = -A\exp\left(-x^2/s^2\right) + \psi\frac{x}{L}, \qquad (3)$$

where A is the depth of the single-ion energy profile; s is the half-width of this profile. The second term describes the transmembrane electrostatic potential in the linear approximation.

The ion-ion electrostatic interactions in our model are approximated by the shielded Coulomb potential

$$V(r) = \frac{b}{r}\exp\left(-\frac{r}{d}\right), \qquad (4)$$

where d is the shielding constant; and b is the constant, which converts the electrostatic energy to the $k_{\mathrm{B}}T$ units. This interaction should be considered as the simplest reasonable approximation of the real ion-ion interaction inside the pore. The empirical constant d allows us to vary the amount of screening.

The values of empirical constants are as follows: $b = 566.2$, $s = 9$ Å, and $L = 20$ Å [15, 18]. The free parameters A and d are varied. The configurations up to $M = 4$ were considered to cover the whole range of possible pore occupancies.

It is easy to deduce that the concerted motion of ions corresponds to some pre-defined "optimal" trajectory in the n-dimensional configurational space. The selected region of the configurational space, where the most probable trajectories are located, obviously corresponds to a deep and rather narrow "groove" in U_n. Figures 1 and 2,*b*,*c* show the examples of such grooves for $n = 2, 3$. If the groove is deep enough, then the probability density $\phi^{(n)}(x_1, \ldots, x_n, t)$ is negligible outside the groove.

Let us define the groove axis, which corresponds to the groove bottom. The groove axis connects the points $M_1 = \{-L, x_2', .., x_n'\}$ and $M_2 = \{x_1'', .., x_{n-1}'', L\}$ located at the "input" and "output" facets of $G^{(n)}$, which correspond to $x_1 = -L$ and $x_n = L$, respectively. M_1 and M_2 are defined as $\frac{\partial U_n(-L, x_2, .., x_n)}{\partial x_i} = 0$, $i = 2, .., n$ and $\frac{\partial U_n(x_1, .., x_{n-1}, L)}{\partial x_i} = 0$, $i = 1, .., n-1$, respectively.

The axis can be parametrized by the length of the curve ξ_1 measured from M_1 toward M_2 as

$$\frac{d\mathbf{r}(\xi_1)}{d\xi_1} = \boldsymbol{\tau}^{(1)}(\xi_1), \tag{5}$$

where $\mathbf{r}(\xi_1) = \sum\limits_{i=1}^{n} x_i^{(r)}(\xi_1)\mathbf{e}^{(i)}$ is the radius-vector of a particular axis point, $x_i^{(r)}(\xi_1)$ are the Cartesian coordinates of this point, $\mathbf{e}^{(i)}$ are the orts of the laboratory coordinate system; and

$$\boldsymbol{\tau}^{(1)} = \frac{\sum\limits_{i=1}^{n} \left|\frac{\partial U_n(\mathbf{x})}{\partial x_i}\right| \mathbf{e}_i}{\sqrt{\sum\limits_{i=1}^{n} \left(\frac{\partial U_n(\mathbf{x})}{\partial x_i}\right)^2}} \tag{6}$$

is a vector tangential to the groove axis.

It is convenient to describe the motion inside the groove in its own local coordinate system, which defines the directions parallel and perpendicular to the groove axis. The parallel direction is given by $\boldsymbol{\tau}^{(1)}$, while $n-1$ remaining perpendicular directions lie in the hyperplane $\mathbb{N}(\xi_1)$, which is normal to $\boldsymbol{\tau}$ in a particular point $\xi_1$of the groove axis. $\mathbb{N}(\xi_1)$ is defined as

$$\left(R(\mathbf{x}) - \mathbf{r}(\xi_1), \boldsymbol{\tau}^{(1)}(\xi_1)\right) = 0, \tag{7}$$

where $R(\mathbf{x})$ is an arbitrary point, which belongs to this hyperplane. Equation (7) can be rewritten as

$$\sum_{i=1}^{n} \left[x_i - x_i^{(r)}(\xi_1)\right] \left|\frac{\partial U_n(\mathbf{x})}{\partial x_i}\right| = 0. \tag{8}$$

Let us define the system of $n-1$ orthonormalized vectors in $\mathbb{N}(\xi_1)$ as

$$\boldsymbol{\tau}^{(\alpha)}(\xi_1) = \sum_{i=1}^{n} \tau_i^{(\alpha)}(\xi_1)\mathbf{e}^{(i)}, \tag{9}$$

where $\alpha = 2, .., n$. Equations (9) and (6) define a full orthonormal local coordinate system at each point of the groove axis. This system is valid in some small vicinity of the groove axis, which ensures that the hyperplanes $\mathbb{N}(\xi_1)$ and $\mathbb{N}(\xi_2)$ of any two points do not intersect. The correspondence between the points $\mathbf{x}$ and $\mathbf{x}^{(r)}$ in the laboratory and local coordinate systems is given by

$$x_i(\boldsymbol{\xi}) = x_i^{(r)}(\xi_1) + \sum_{\alpha=2}^{n} \xi_\alpha \tau_i^{(\alpha)}(\xi_1).$$

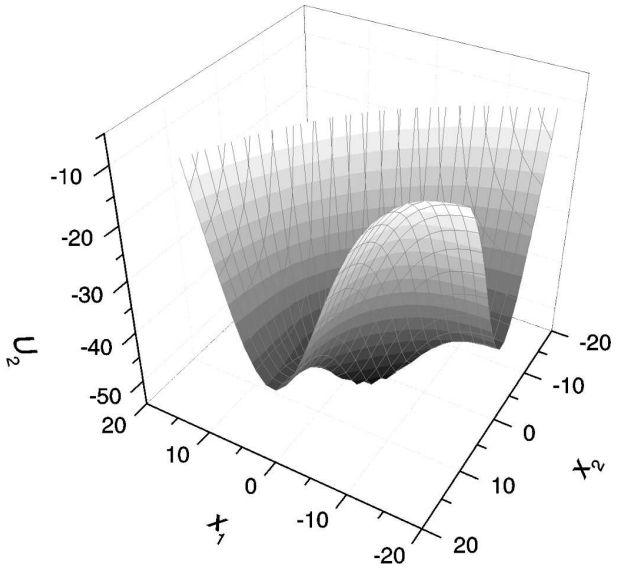

Fig. 1. Surface plot of U_2 for $A = 40k_{\mathrm{B}}T$, $d = 5$ Å. The groove is clearly visible

Potential (2) can be rewritten using the local coordinates $\boldsymbol{\xi} \equiv \{\xi_\alpha\}$, $\alpha = 1, .., n$ as

$$\tilde{U}_n(\boldsymbol{\xi}) \equiv U_n\left[\mathbf{r}(\xi_1) + \sum_{\alpha=2}^{n} \xi_\alpha \boldsymbol{\tau}^{(\alpha)}(\xi_1)\right]. \tag{10}$$

The criterion for the existence of a groove can be formalized easily as

$$\left.\frac{\partial \tilde{U}_n(\boldsymbol{\xi})}{\partial \xi_\alpha}\right|_{\xi_\alpha=0} = 0,$$

$$\left.\left|\frac{\partial \tilde{U}_n(\boldsymbol{\xi})}{\partial \xi_1}\right|\right|_{\xi_\alpha=0} \ll \left.\left|\frac{\partial^2 \tilde{U}_n(\boldsymbol{\xi})}{\partial \xi_\alpha^2}\Delta_\alpha(\xi_1)\right|\right|_{\xi_\alpha=0}, \quad \alpha = 2, .., n, \tag{11}$$

where $\alpha = 2, .., n$; $\Delta_\alpha(\xi_1)$ is a characteristic half width of the groove in the direction ξ_α at the point ξ_1. In other words, the "side walls" of the groove are very steep in comparison with the profile of the groove bottom. It is also implied implicitly that the groove is deep enough.

2.3. Superions

As was already mentioned in Introduction, the general theory of the multiparticle diffusion in a narrow pore developed in [13] leads to the system of multidimensional Fokker–Planck equations

$$\frac{\partial \phi^{(n)}(x_1, \ldots, x_n, t)}{\partial t} = D\sum_{i=1}^{n} \frac{\partial}{\partial x_i} \times$$

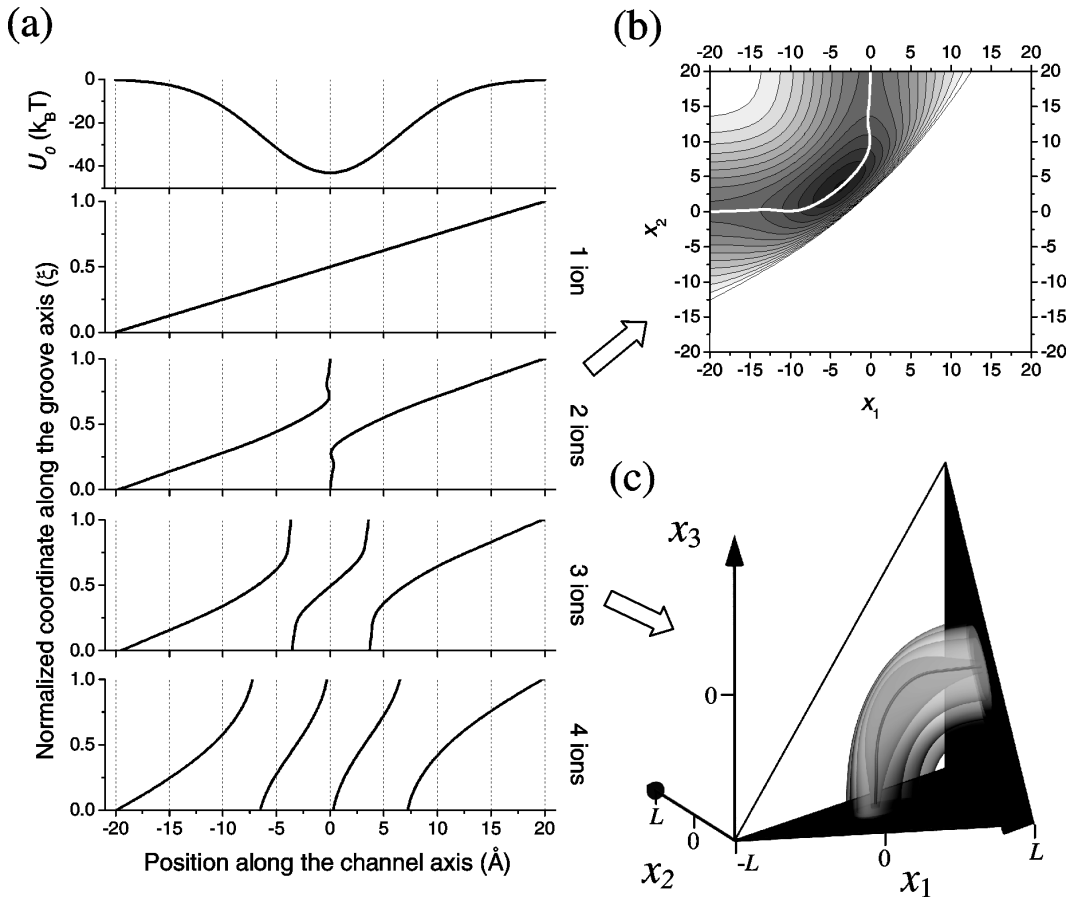

Fig. 2. Groove axis in various occupancy states for $A = 43k_BT$, $d = 3$ Å. *a*) The parametric coordinates of the groove axis for $n = 1,..,4$. The i-th curve in each particular panel (counting from the left) corresponds to the coordinate $x_i(\xi)$ of the groove axis. The coordinate ξ is normalized for clarity. Top panel shows the single-ion energy profile for the reference. *b*) The contour plot of the potential U_2 (two ions in the channel) with the groove axis superimposed as a white line. *c*) The plot of the isosurfaces of the three-dimensional potential U_3 (three ions in the channel). The isosurfaces are drawn at $-66k_BT$, $-60k_BT$, $-54k_BT$ and $-50k_BT$ counting from inside out. The groove axis is shown as a solid line inside the isosurfaces

$$\times \left[\frac{\partial U_n(x_1,\ldots,x_n)}{\partial x_i} \phi^{(n)}(\mathbf{x},t) + \frac{\partial \phi^{(n)}(x_1,\ldots,x_n,t)}{\partial x_i} \right], \tag{12}$$

where $\phi^{(n)}(x_1,\ldots,x_n,t)$ is the probability density in the case of exactly n ions in the pore, and D is the diffusion coefficient. Equations (12) are supplemented by the boundary conditions (1), which form the hierarchical sequence of equations of the growing dimensionality.

The local coordinate system $\{\xi_i\}$ is curvilinear, but their Lame coefficients are all equal to 1:

$$H_\alpha = \sqrt{\sum_{i=1}^{n} \left(\frac{\partial x_i}{\partial \xi_\alpha} \right)^2} = \sqrt{\sum_{i=1}^{n} \left[\tau_i^{(\alpha)}(\xi_1) \right]^2} = 1.$$

This makes rewriting Eq. (12) in terms of $\{\xi_i\}$ trivial:

$$\frac{\partial \tilde{\phi}^{(n)}(\boldsymbol{\xi};t)}{\partial t} =$$

$$= D \left\{ \frac{\partial}{\partial \xi_1} \left[\frac{\partial \tilde{U}_n(\boldsymbol{\xi})}{\partial \xi_1} \tilde{\phi}^{(n)}(\boldsymbol{\xi};t) + \frac{\partial \tilde{\phi}^{(n)}(\boldsymbol{\xi};t)}{\partial \xi_1} \right] + \right.$$

$$\left. + \sum_{\alpha=2}^{n} \frac{\partial}{\partial \xi_\alpha} \left[\frac{\partial \tilde{U}_n(\boldsymbol{\xi})}{\partial \xi_\alpha} \tilde{\phi}^{(n)}(\boldsymbol{\xi};t) + \frac{\partial \tilde{\phi}^{(n)}(\boldsymbol{\xi};t)}{\partial \xi_\alpha} \right] \right\}, \tag{13}$$

where

$$\tilde{\phi}^{(n)}(\boldsymbol{\xi};t) = \phi^{(n)} \left[\mathbf{r}(\xi_1) + \sum_{\alpha=2}^{n} \xi_\alpha \boldsymbol{\tau}^{(\alpha)}(\xi_1); t \right]. \tag{14}$$

The first term of Eq. (13) describes the slow relaxation along the groove, while the second term describes the very fast relaxation in the perpendicular cross section of the groove. We are only interested in the slow phase, which determines all macroscopic characteristics of the pore. Therefore, we can consider the system in the adiabatic approximation. At the times larger than the characteristic relaxation time in the perpendicular cross-section of the groove, the distribution function $\tilde{\phi}^{(n)}$ is in local equilibrium in any hyperplane $\mathbb{N}(\xi_1)$. As a result, the solution of (13) can be written as

$$\tilde{\phi}^{(n)}(t;\boldsymbol{\xi}) = \varphi^{(n)}(t;\xi_1)\frac{e^{-\tilde{U}_n(\boldsymbol{\xi})}}{z_n(\xi_1)}, \tag{15}$$

where

$$z_n(\xi_1) = \int\limits_{-\Delta_2}^{\Delta_2} d\xi_2, .., \int\limits_{-\Delta_n}^{\Delta_n} d\xi_n e^{-\tilde{U}_n(\boldsymbol{\xi})}. \tag{16}$$

The limits of integration Δ_i are chosen to ensure that $z_n(\xi_1)$ is independent of Δ_i. It is obvious that approximation (15) approaches the exact solution with increase in the depth and with decrease in the width of the groove.

The substitution of (15) into (13) and the integration over the same variable and in the same limits as in Eq. (16) yield

$$\frac{\partial\varphi^{(n)}(t;\xi_1)}{\partial t} =$$

$$= D\frac{\partial}{\partial\xi_1}\left[\frac{\partial U_n^{\text{eff}}(\xi_1)}{\partial\xi_1}\varphi^{(n)}(t;\xi_1) + \frac{\partial\varphi^{(n)}(t;\xi_1)}{\partial\xi_1}\right], \tag{17}$$

where

$$U_n^{\text{eff}}(\xi_1) = \int\limits_{-\Delta_2}^{\Delta_2} d\xi_2, .., \int\limits_{-\Delta_n}^{\Delta_n} d\xi_n \frac{\partial\tilde{U}_n(\boldsymbol{\xi})}{\partial\xi_1}\frac{e^{-\tilde{U}_n(\boldsymbol{\xi})}}{z_n(\xi_1)} =$$

$$= -\ln z_n(\xi_1) \tag{18}$$

is a local free energy in each hyperplane $\mathbb{N}(\xi_1)$ called an effective potential.

Equation (17) is essentially a one-dimensional Fokker–Planck equation for a collective quasiparticle, which moves along the groove axis in the effective potential (18). We will call this quasiparticle a *superion* hereafter. It is necessary to emphasize that the superion moves along the curved one-dimensional groove axis in the n-dimensional configurational space, while the real ions move along a pore axis in the real space.

The approximated steady-state solution of (13) can be written in terms of superions as

$$\tilde{\phi}^{(n)}(\boldsymbol{\xi}) = \begin{cases} \varphi^{(n)}(\xi_1)\frac{e^{-\tilde{U}_n(\boldsymbol{\xi})}}{z_n(\xi_1)}, & \boldsymbol{\xi}\in\Re^{(n)}, \\ 0, & \boldsymbol{\xi}\notin\Re^{(n)}, \end{cases} \tag{19}$$

where $\Re^{(n)}$ is a part of the configurational space inside the groove (determined by the integration limits Δ_i in Eq. (16)); and $\varphi^{(n)}(\xi_1)$ is the steady-state solution of Eq. (17). This approximation is very close to the exact solution if the groove is deep enough (more than several $k_{\text{B}}T$), and Eq. (11) is satisfied.

2.4. Macroscopic characteristics of the pore

In order to compute the macroscopic characteristics of the pore, it is convenient to subdivide the probability density $\varphi^{(n)}(\xi_1)$ into the known equilibrium and unknown non-equilibrium parts, as it was done in the general theory [13]:

$$\tilde{\phi}^{(n)}(\boldsymbol{\xi}) \equiv e^{-\tilde{U}_n(\boldsymbol{\xi})}v^{(n)}(\boldsymbol{\xi}), \tag{20}$$

where $v^{(n)}$ is related to the local entropy, which is constant under equilibrium conditions [13]. All macroscopic characteristics of the pore can be expressed in terms of v. Equation (19) can be written as

$$\nu^{(n)}(\boldsymbol{\xi}) = \nu^{(n)}(\xi_1) = \begin{cases} \frac{\varphi^{(n)}(\xi_1)}{z_n(\xi_1)}, & \boldsymbol{\xi}\in\Re^{(n)}, \\ 0, & \boldsymbol{\xi}\notin\Re^{(n)}. \end{cases} \tag{21}$$

Equation (17) in the steady state transforms to the following simple equation for v:

$$\frac{d}{d\xi_1}\left[e^{-U_n^{\text{eff}}(\xi_1)}\frac{d\nu^{(n)}(\xi_1)}{d\xi_1}\right] = 0. \tag{22}$$

The boundary conditions of Eq. (22) are obtained from Eq. (1) using relation (20):

$$\begin{aligned} v^{(n)}(0) &= r_1 v^{(n-1)}(0), \\ v^{(n)}(l_n) &= r_2 v^{(n-1)}(l_{n-1}), \end{aligned} \tag{23}$$

where $r_{1,2} \equiv c_{1,2}e^{U_0(\mp L)}$, l_n is the length of the groove axis in the case of n ions in the pore.

Equation (22) is one-dimensional for any number of ions in the pore and can be solved analytically:

$$\nu^{(n)}(\xi_1) = \nu^{(n)}(0) + \left[\nu^{(n)}(l_n) - \nu^{(n)}(0)\right]\times$$

$$\times \int_0^{\xi_1} e^{U_n^{\text{eff}}(\xi')} d\xi' \Bigg/ \int_0^{l_n} e^{U_n^{\text{eff}}(\xi')} d\xi'.$$

Thus, we obtained *analytical* solutions for all occupancy states of the pore. The only quantities, which should be computed numerically, are the effective potentials $U_n^{\text{eff}}(\xi_1)$.

The probabilities of occupancy states are obtained in the general theory developed in [13] as

$$w_n = \frac{\frac{p^{(n)}}{n!}}{\sum\limits_{m=0}^{n_{\max}} \frac{p^{(m)}}{m!}}, \tag{24}$$

where $p^{(n)} = \int\limits_{-L}^{L} dx_1, ..., \int\limits_{-L}^{L} dx_n \phi^{(n)}(x_1, \ldots, x_n, t)$ is the norm of $\phi^{(n)}(x_{i_1}, \ldots, x_{i_n}, t)$.

Using Eqs. (24) and (21), we can write the probabilities of occupancy states of the pore as

$$w_n = \frac{q^{(n)}}{\sum\limits_{i=0}^{M} q^{(n)}}, \tag{25}$$

where $q^{(n)} = \int\limits_0^{l_n} d\xi_1 z_n(\xi_1) v^{(n)}(\xi_1)$.

The charge density along the pore can be obtained using Eq. (22) from work [13] and Eq. (21):

$$\rho^{(n)}(z) = \frac{1}{q^{(n)}} \sum_{i=1}^{n} \Bigg\{ \int_{-L}^{L} dx_1, .., \int_{-L}^{L} dx_{i-1} \times$$

$$\times \int_{-L}^{L} dx_{i+1}, .., \int_{-L}^{L} dx_n e^{-U_n(x_1,..,x_{i-1},z,x_{i+1},..,x_n)} \times$$

$$\times \left[\nu^{(n)} \left[\xi_1 \left(x_1, .., x_{i-1}, z, x_{i+1}, .., x_n \right) \right] \right] \Bigg\}. \tag{26}$$

Finally, the current through the pore in the occupancy state n is obtained using Eq. (18) and Eq. (25) from [13], which defines the current through the given cross section of the channel in the given occupancy state:

$$J^{(n)}(\xi_1) = -n \frac{D}{q^{(n)}} e^{-U_n^{\text{eff}}(\xi_1)} \frac{\partial v^{(n)}(\xi_1)}{\partial \xi_1}. \tag{27}$$

The stationary current is obviously independent of ξ_1. Thus, any value of $\xi_1$can be used. The total current through the pore is

$$J = \sum_{i=1}^{M} w_n J^{(n)}(\xi_1) \Big|_{\xi_1 = 0}. \tag{28}$$

The stationary current can also be expressed in the integral form by rewriting Eq. (27) with the use of the boundary conditions (1) and Eq. (20):

$$J^{(n)} = -n \frac{D}{q^{(n)}} \left[c_1 \tilde{\phi}^{(n-1)}(x_2', .., x_n') e^{U_n^{\text{eff}}(0)} - \right.$$

$$\left. - c_2 \tilde{\phi}^{(n-1)}(x_1'', .., x_{n-1}'') e^{U_n^{\text{eff}}(l_n)} \right] \Bigg/ \int_0^{l_n} e^{U_n^{\text{eff}}(\xi_1)} d\xi_1. \tag{29}$$

2.5. Numerical solution

The groove axis is found numerically using Eq. (5) in conjunction with constrained energy minimization, which suppresses possible inaccuracies in finding the bottom of the groove. Once the groove axis is found, the orthonormal perpendicular vectors (9) are computed at each discrete point. The rectangular grid is then defined in the hyperplane $\mathbb{N}$, and z_n is computed by the direct multidimensional integration according to Eq. (16). Once z_n are known at each discrete point of the groove axis, the computations of v_n and the macroscopic properties of the pore are trivial. This algorithm is implemented in the custom program written in FORTRAN 90.

3. Results

3.1. The groove axis in different occupancy states

Figure 2,*a* shows the grooves in the potentials U_n for $n = 1, .., 4$. It is clearly seen that the positions of the ions change in a concerted way along the groove axis. Figures 2,*b* and 2,*c* visualize the groove axis in two- and three-dimensional spaces. It is visible that the axis connects the input and output facets and is surrounded by the "onion shells" of the isolines of U_n.

3.2. Effective potentials

Figure 3 shows the effective potential U_n^{eff} for $n = 1, .., 4$. The depth of the effective potential reduces with increase

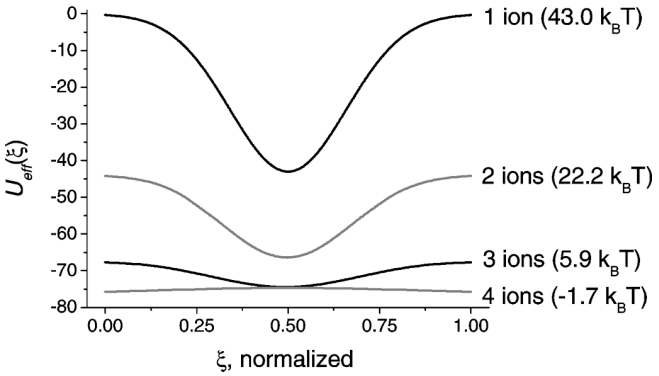

Fig. 3. Effective potentials for various channel occupancies for $A = 43k_BT$, $d = 3$ Å. The depths of the potentials are shown in parentheses (negative depth corresponds to the energy barrier). The parameters are the same as in Fig. 1

in n and reaches approximately 6 k_BT for the last stable configuration of ions ($n = 3$ for given parameters). The configuration with 4 ions introduces a small energy barrier to the effective potential.

The dramatic decrease of the depth of effective potentials in comparison with U_0 clearly shows the physical reason for the multiple pore occupancy. Indeed, the collective superions, which move in the very shallow effective potential, facilitate a much larger current though the channel than individual ions, which move in the single-ion potential U_0.

3.3. Comparison with the generic computational procedure

The approximation of superions itself and the general analytical theory built in [13] are robust and correct. However, the generic computational procedure (referred as GCP hereafter), which was developed in [13], is rather inaccurate. The numerical solution in GCP is correct in equilibrium; however, the inaccuracy increases with non-equilibrium factors. The integral characteristics, such as w_n, are expected to be quite accurate near the equilibrium, while the currents $J(n)$ can only be treated qualitatively. Thus, the approximation of superions can be validated against the GCP using w_n, near the equilibrium. Figure 4,*a* shows the concentration dependences of the channel occupancies w_n and the mean number of ions in the channel in equilibrium.

Figure 4,*b* shows the difference in the mean occupancies computed in the GCP and in the approximation of the superions. There is the almost ideal correspondence between the concentration dependences in equilibrium, but the results diverge consistently with increase in the membrane potential. The difference remains very small

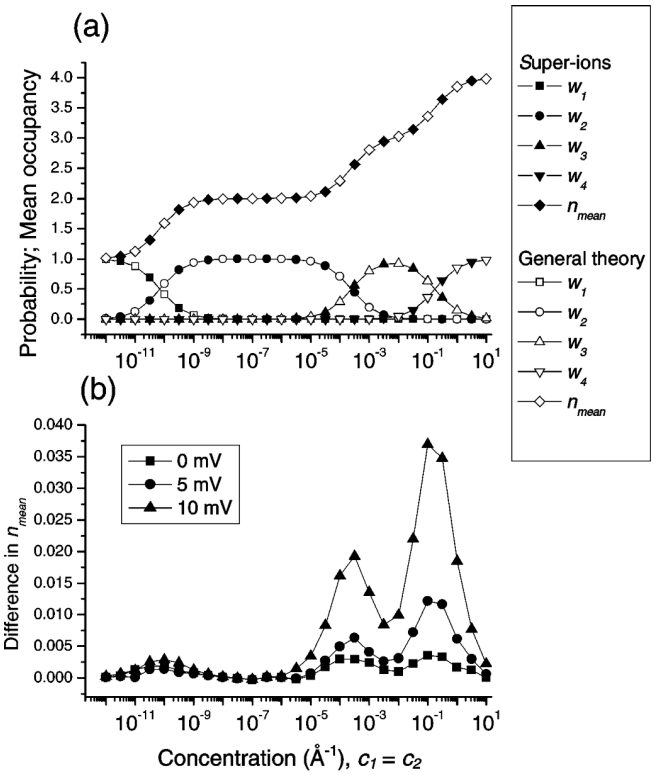

Fig. 4. *a*) Concentration dependences of the mean occupancy n_{mean} and the occupancy probabilities w_n in the approximation of superions and in the general theory for $\psi = 0$ mV. The parameters are the same as in Fig. 2. *b*) The difference in n_{mean} computed in the GCP and in the approximation of superions for various values of ψ

(less than 1.5%) up to $\psi = 10$ mV. Maximal deviations are observed in the transition regions between different occupancy states. The magnitudes of these deviations increase with the occupancy. The comparison for larger values of ψ is not justified due to uncontrollable numerical errors in GCP.

3.4. Current-voltage relationships

Figure 5,*a* shows the current-voltage relationships for different concentrations in the approximation of superions computed using Eq. (29). The current increases exponentially for small voltages, while the parts corresponding to large voltages are linear or slightly saturating. The curves for different concentrations eventually converge for the very large voltages.

The shape of the current-voltage relationships reflects a complex interplay between the contributions of different occupancy states. This can be illustrated by comparing the current-voltage relationships (Fig. 5,*a*) with the

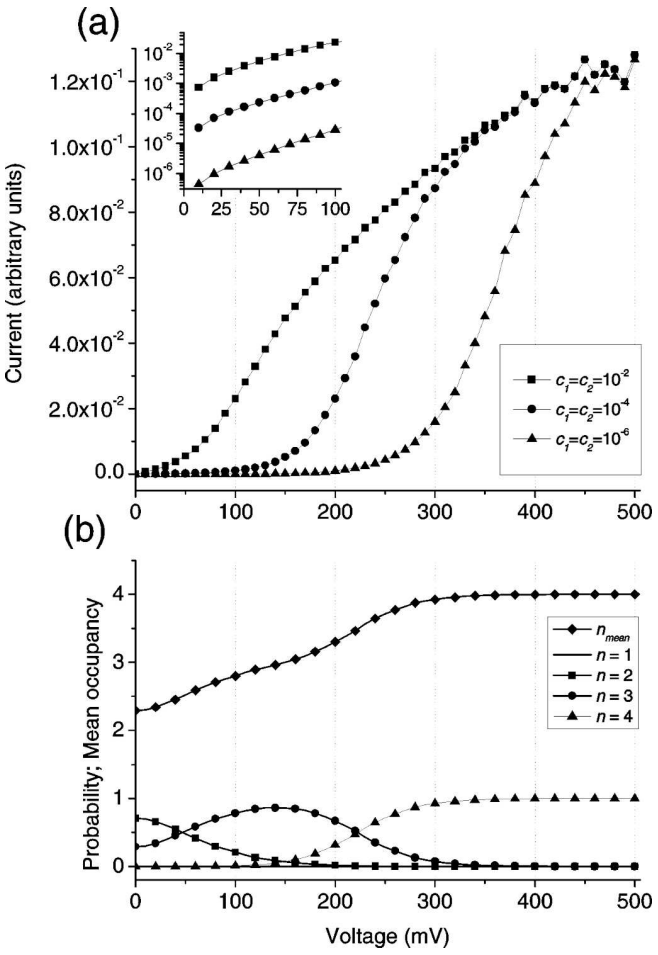

Fig. 5. *a*) Current-voltage relationships for indicated values of concentrations (in $Å^{-1}$ units) in the approximation of superions. Inset shows the region of small voltages on the log scale to emphasize the exponential shape of the curves. *b*) Voltage dependences of the mean occupancy n_{mean} and the occupancy probabilities w_n for $c_1 = c_2 = 10^{-4}$ $Å^{-1}$(corresponds to the middle curve in (*a*)). The parameters are the same as in Fig. 2

dependences of w_n and the mean occupancy on the voltage (Fig. 5,*b*). When the dominant occupancy reaches the maximal number of ions (four in our case), the transition to the linear part begins. In the linear regime, the pore is saturated with ions completely, so the current becomes almost independent of the concentrations. As a consequence, all curves in Fig. 5,*a* converge for very large voltages.

4. Discussion

In the present work, the concept of the superion is introduced. It is based on a specific shape of U_n, which possesses a well-defined deep groove corresponding to the most preferable path of multiple ions through the channel. The existence of the deep groove is the only additional assumption in comparison to the general theory. The motion of the superions for different occupancies is described by the system of one-dimensional Fokker–Planck equations, which are coupled by simple hierarchical boundary conditions (23).

It is important to validate our approximation against the general theory. The multidimensional equations of the general theory are currently solved numerically by means of a generic computational procedure, which produces semiquantitative results. Due to these numerical issues, the comparison is currently limited to integral properties and to small deviations from equilibrium. It is shown that the approximation of superions reproduces the occupancy states w_n extremely well. This means that the probability of finding the system outside the groove is indeed negligible.

The approximation of superions can also be a practical way of computing the current and other macroscopic properties of the channel, which are very hard to obtain accurately using the generic computational procedure. In contrast to the generic computational procedure, the computations are very accurate and very cheap. This makes our technique preferable for all potentials, where the well-defined groove exists.

The approximation of superions provides the theoretical description of the well-known mechanism of the so-called "barrier-less knock-on conductance" in ion channels [2, 18]. Indeed, it is shown that the depths of effective potentials for the superions become smaller with increase in the occupancy. The potential for the highest stable occupancy is always almost "flat" even if the depth of the initial single-ion potential is 50–100$k_{\mathrm{B}}T$ (Fig. 3). Thus, the corresponding superion moves almost freely inside the groove and facilitates the conductance.

5. Conclusion

The general theory of the single-file multiparticle diffusion in narrow pores developed in [13] can be greatly simplified in a rather wide class of specific shapes of single-ion energy profiles. In such potentials, the ions move in a highly concerted manner, which corresponds to the existence of a narrow deep groove in the energetic landscape. The motion of multiple ions can be reduced to the motion of a single quasiparticle (the superion), which moves in the one-dimensional effective potential along the groove. It is shown that the effective potentials of superions, which correspond to the conducting occupancies of the channel, are essentially flat. This ex-

plains the phenomenon of the barrierless conduction in narrow channels with multiple occupancy in a very elegant way. The approximation of superions also reduces the computational complexity of the problem dramatically in comparison with the generic computational procedure.

1. D.A. Doyle *et al.*, Science **280**, 69 (1998).
2. S. Berneche and B. Roux, Nature **414**, 73 (2001).
3. B. Hille, *Ion Channels of Excitable Membranes*(Sinauer Associates, Sunderland, Mass., 2001).
4. G. Hummer, J.C. Rasaiah, and J.P. Noworyta, Nature **414**, 188 (2001).
5. F. Zhu and K. Schulten, Biophys. J. **85**, 236 (2003).
6. D.J. Mann and M.D. Halls, Phys. Rev. Lett. **90**, 195503 (2003).
7. S. Berneche and B. Roux, Biophys. J. **78**, 2900 (2000).
8. S.-H. Chung, T.W. Allen, and S. Kuyucak, Biophys. J. **82**, 628 (2002).
9. M. Compoint *et al.*, Biochem. Biophys. Acta **1661**, 26 (2004).
10. S. Chang *et al.*, Biophys. J. **77**, 2517 (1999).
11. B. Corry, S. Kuyucak, and S.-H. Chung, Biophys. J. **78**, 2364 (2000).
12. A. Aksimentiev and K. Schulten, Biophys. J. **88**, 3745 (2005).
13. V.N. Kharkyanen and S.O. Yesylevskyy, Phys. Rev. E **80**, 031118 (2009).
14. R.J. Mashl *et al.*, Biophys. J. **81**, 2473 (2001).
15. S.O. Yesylevskyy and V.N. Kharkyanen, Phys. Chem. Chem. Phys., 3111 (2004).
16. P. McGill and M.F. Schumaker, Biophys. J. **71**, 1723 (1996).
17. W. Stephan, B. Kleutsch, and E. Frehland, J. of Theor. Biol. **105**, 287 (1983).
18. S.O. Yesylevskyy and V.N. Kharkyanen, Chem. Phys. **312**, 127 (2004).
19. B. Hille and W. Schwarz, J. Gen. Physiol. **72**, 409 (1978).

Received 04.01.11

СУПЕРІОНИ У ВУЗЬКИХ НАНОПОРАХ З МНОЖИННОЮ ЗАСЕЛЕНІСТЮ

В.М. Харкянен, С.О. Єсилевський, Н.М. Березецька

Р е з ю м е

Загальну теорію однорядної багаточастинкової дифузії у вузьких порах можна суттєво спростити у випадку одночастинкового потенціального профілю у формі перевернутого дзвона, який часто спостерігається у біологічних іонних каналах. Такий профіль приводить до появи вузького та глибокого жолоба в енергетичному ландшафті системи, який відповідає оптимальному шляху провідності у конфігураційному просторі. Якщо такий жолоб існує, то рух кількох частинок можна звести до руху єдиної квазічастинки, названої суперіоном, яка переміщується у одновимірному ефективному потенціалі. Концепція суперіонів значно зменшує обчислювальну складність задачі та дає просту й наочну фізичну інтерпретацію феноменів провідності у вузьких нанопорах.